IGARSS 2023 - 2023 IEEE International Geoscience and Remote Sensing Symposium | 979-8-3503-2010-7/23/$31.00 ©2023 IEEE | DOI: 10.1109/IGARSS52108.2023.10282271

DESPECKLING OF MULTIFREQUENCY SAR DATA USING ELECTROMAGNETIC SCATTERING MODELS

Gerardo Di Martino, Alessio Di Simone, Antonio Iodice, Daniele Riccio, Giuseppe Ruello

University of Naples Federico II
Department of Electrical Engineering and Information Technology

ABSTRACT

Interpretation and processing of synthetic aperture radar (SAR) imagery is negatively affected by speckle noise, that can be faced by proper despeckling pre-processing. In this work, we propose a simple approach for the despeckling of multi-frequency SAR data under the hypotheses that they are relevant to bare soil surfaces and that are acquired by the same sensor, e.g., AIRSAR. The proposed approach is based on a frequency-compensation step, where the dependence of the signal strength upon operating frequency is compensated by means of surface scattering model suited to natural surfaces. Once such a pre-processing step is carried out, any despeckling filter suited to SAR time series filtering can be applied. Quantitative indicators evaluated on both simulated and actual SAR data reveal the benefits of the proposed compensation step w.r.t. pure multitemporal and single-channel filtering.

Index Terms— SAR, speckle filtering, multi-frequency, scattering

1. INTRODUCTION

SAR despeckling is a hot research topic that has been attracting much interest in the radar and remote sensing communities [1]. Most research efforts have been focusing on filtering single-channel data, while the launch of the ESA Sentinel-1 mission has stimulated great efforts in the development of filters for multi-temporal SAR imagery [2], [3]. In the more general context of multi-dimensional SAR data processing, despeckling of multi-frequency SAR data has been the subject of very few works, e.g., [4], [5].

However, numerous applications could effectively take advantage of multi-frequency SAR data processing, e.g., study and analysis of land cover types [6], classification [7] and snow cover analysis [8].

Speckle noise affecting multi-frequency data could be simply faced by applying any single-channel despeckling filter to each band separately. However, it is reasonable to expect that a multi-dimensional filtering approach where all image bands are jointly filtered leads to improved speckle rejection. Actually, such considerations have motivated the development of techniques for multi-temporal SAR despeckling [2]. Here we propose a simple approach to jointly filter multi-frequency SAR data acquired over bare soil surfaces with multi-frequency SAR sensors, such as the NASA AIRSAR, SIR-C/X-SAR, and the upcoming NASA-ISRO SAR Mission (NISAR). The proposed approach is based on a frequency-calibration procedure which makes use of scattering models adequate to bare soil surfaces for compensating the dependence of SAR data upon the operating frequency.

2. ELECTROMAGNETIC SCATTERING MODEL

In this paper, a bare soil surface is described by means of the fractal geometry, which has been widely recognized as the best tool to describe self-similarity and self-affinity of natural land surfaces [9].

More specifically, the surveyed surface roughness is modelled as a two-dimensional (2D) fractional Brownian motion (fBm) process, i.e., a 2-D stochastic process $z(x,y)$ whose increments $z(x,y) - z(x',y')$ over a fixed horizontal distance $\tau = \sqrt{(x-x')^2 + (y-y')^2}$ are zero-mean Gaussian random variables with standard deviation $T^{1-H}\tau^H$, T being the topothesy, measured in [m], and H being the Hurst coefficient, with $0<H<1$, related to the surface fractal dimension $D = 3 - H$.

In this work, electromagnetic scattering from bare soil surfaces is described by means of the Small Perturbation Method (SPM), as it expresses the backscattering coefficient through straightforward analytical equations and exhibits validity limits which are suited to SAR imagery.
Under SPM, the backscattering coefficient of the surveyed scene reads as [10]

$$\sigma^0_{pq}(k) = 2\pi 8 k^{2-2H} \cos^4\theta \left|\beta_{pq}\right|^2 \frac{S_0}{(2\sin\theta)^{2+2H}} \qquad (1)$$

where the subscripts p and q indicate the receive and transmit polarization channels, respectively; θ is the local incidence angle, k is the electromagnetic wavenumber, β_{pq} is a function of the signal polarization, the complex dielectric constant ε_r of the surface and the local incidence angle; finally, S_0, which is related to T and H [10], describes the

spectral behavior of the fBm surface and is measured in $[m^{(-2-2H)}]$.

3. MULTI-FREQUENCY SAR DESPECKLING

The observed noisy SAR image intensity I relevant to the wavenumber k_m is expressed via the following image model

$$I(k_m) = \sigma^0_{pq}(k_m) A_{cell}\, n \quad , \quad m = 1, \dots, M \qquad (2)$$

where A_{cell} is the resolution cell area, n denotes the speckle noise, M is the number of available frequencies.

To jointly reduce speckle noise in the multi-frequency dataset, all bands are normalized to a common reference wavenumber k_0. Accordingly, the following normalization is performed:

$$I_m(k_0) = I(k_m) \frac{k_0^{2-2H}}{k_m^{2-2H}} = \sigma^0_{pq}(k_0) A_{cell}\, n \quad , \quad m = 1, \dots, M \qquad (3)$$

The normalized SAR image series I_m (m = 1,…, M) can be regarded as the series of M measurements of the scene reflectivity at wavenumber k_0. As a result, any multi-temporal despeckling filter can then be applied to obtain the filtered data.

Finally, the original intensity data dynamic can be restored by inverting (3).

It is worth mentioning that the normalization procedure in (3) requires estimation of the Hurst coefficient over the whole illuminated surface; to this end, the algorithm in [11] might be applied before filtering in order to retrieve the H map from the noisy images. However, for most natural surfaces and multi-temporal filters it is reasonable to assume H constant within the search window of the algorithm (whose linear size is typically of few tens of pixels), and, hence, a reference value can be used for H. Typical values of H for natural surfaces range from 0.55 to 0.95 [12]. Similarly, the dependence of the dielectric constant upon frequency can be neglected as long as it can be assumed homogeneous within the search window.

4. RESULTS

4.1. Simulation Results

Here we present simulation results relevant to the fBm surface and multi-frequency SAR sensor defined in Table 1. For the sake of conciseness only results relevant to C-band are shown in Fig. 1, where ratio image, i.e., the ratio between the noisy image and the corresponding filtered one is shown for despeckling filters. Table 2 includes some synthetic quality indicators, namely mean of image (MoI), coefficient of variation (Cx), and despeckling gain (DG), which are defined e.g. in [3]. The quality indicators have been averaged over the 4 bands simulated.

Table 1. Simulation parameters

Parameter	Symbol	Value
Hurst coefficient	H	0.8
Topothesy	T	0.005 m
Dielectric constant	ε_r	10
Viewing angle	θ	30°
Frequency	f_m	[1.20, 3.20, 5.40, 9.60] GHz
Polarization	pq	VV
Azimuth resolution	Δx	1 m
Range resolution	Δr	1 m

Table 2. Performance Parameters – Simulation Test Case

	MoI	C_x	DG
Noisy	39.76	1.99	0
Reference	39.86	1.23	∞
Proposed	39.07	1.23	9.43
Single-channel	38.46	1.08	7.07
Multi-temporal	38.87	1.24	8.96

The proposed despeckling approach based on frequency compensation [Fig. 1(c)] is compared with both single-channel filtering, i.e., independent filtering of each band [Fig. 1(d)] and pure multi-temporal filtering, i.e., without frequency compensation [Fig. 1(e)]. For single- and multi-channel filtering, here we make use of SARBM3D and MSARBM3D filters, respectively [2]. The introduction of the frequency-normalization procedure leads to enhanced despeckling capabilities as it is evident from both the synthetic indicators in Table 2 and the ratio images in Fig. 1.

4.2. Results on Real Data

Here we apply the proposed normalization procedure to a real AIRSAR image acquired on Flevoland on June 15, 1991. The multi-frequency image comprises P-band (0.45 GHz), L-band (1.26 GHz), and C-band (5.31 GHz) data. Figs. 2-4 show the noisy 512x512 HH subset images used as input along with the despeckling results obtained with the proposed approach, pure multi-temporal, and single-channel filtering. Due to the current implementation of MSAR-BM3D, which cannot process 3-band images, here we rely on 2S-PPB [13] as the multi-temporal despeckling algorithm to be applied after the normalization procedure. Accordingly, comparisons are made with this filter and its single-channel filtering counterpart, i.e., PPB [14]. For this test case, we have set H = 0.8 for frequency-normalization purposes. Synthetic no-reference despeckling quality indicators, namely MoI, MoR, and ENL are provided in Table 3. In particular, evaluation of ENL is carried out in the red box shown in Fig. 2(a). The frequency-normalization step leads to more balanced histograms, which, in turn, allow for a better temporal average in 2S-PPB, i.e., a less bias is obtained w.r.t. pure multi-temporal filtering. Additionally, some bright features are better preserved, especially at low frequencies. PPB shows visible edge

Table 3. Performance Parameters – Real Test Case

	MoI			MoR			ENL		
	P-band	L-band	C-band	P-band	L-band	C-band	P-band	L-band	C-band
Noisy	0.0085	0.052	0.20	1	1	1	13.17	11.84	11.36
Proposed	0.0083	0.052	0.20	0.93	0.99	1.04	1427.3	1426.2	1427.2
Single-channel	0.0084	0.052	0.20	0.99	0.98	0.99	692.7	191.9	754.6
Multi-temporal	0.0126	0.089	0.15	0.81	0.72	1.32	1464.5	1440.5	755.4

oversmoothing and widespread artifacts resembling watercolor strokes. Finally, the availability of a larger number of bands allows the proposed approach to achieve a larger ENL w.r.t. single-channel filtering.

5. CONCLUSIONS

In this paper, we present a convenient methodology for speckle reduction in multi-frequency SAR data. The proposed algorithm is based on a pre-processing step where the dependence of SAR intensity upon the operating frequency is compensated by means of surface scattering models suited to bare soil surfaces. As a result each band of the multi-frequency dataset is normalized to a common arbitrary frequency.

To this end, the surveyed scene is modeled through fractal geometry, while SPM is adopted for scattering evaluation. A simple image model is adopted to relate the measured SAR data intensity to the surface backscattering coefficient and then to the surface and sensors parameters.

Once such a frequency-compensation pre-processing step is undertaken, any multi-temporal filter can be applied to the normalized multi-dimensional dataset.

Promising results obtained on both simulated and actual AIRSAR datasets prove the benefits of this simple frequency-compensation step in terms of speckle reduction against single-channel and pure multi-temporal filtering.

Finally, it is worth noting that this work does not deal with coregistration issues that arise when filtering multi-frequency SAR images acquired from different sensors and/or acquisition geometries.

ACKNOWLEDGMENT

This study was carried out within the Agritech National Research Center and received funding from the European Union Next-GenerationEU (PIANO NAZIONALE DI RIPRESA E RESILIENZA (PNRR) – MISSIONE 4 COMPONENTE 2, INVESTIMENTO 1.4 – D.D. 1032 17/06/2022, CN00000022). This manuscript reflects only the authors' views and opinions, neither the European Union nor the European Commission can be considered responsible for them.

REFERENCES

[1] F. Argenti, A. Lapini, T. Bianchi and L. Alparone, "A Tutorial on Speckle Reduction in Synthetic Aperture Radar Images," *IEEE Geosci. Remote Sens. Mag.*, vol. 1, no. 3, pp. 6-35, Sept. 2013.

[2] G. Chierchia, M. El Gheche, G. Scarpa and L. Verdoliva, "Multitemporal SAR image despeckling based on block-matching and collaborative filtering", *IEEE Trans. Geosci. Remote Sens.*, vol. 55, no. 10, pp. 5467-5480, Oct. 2017.

[3] G. Di Martino, A. Di Simone, A. Iodice and D. Riccio, "Benchmarking Framework for Multitemporal SAR Despeckling," *IEEE Trans. Geosci. Remote Sens.*, vol. 60, pp. 1-26, 2022, Art no. 5207826.

[4] J.-S. Lee, M. R. Grunes and S. A. Mango, "Speckle Reduction in Multipolarization, Multifrequency SAR Imagery," *IEEE Trans. Geosci. Remote Sens.,* vol. 29, no. 4, pp. 535-544, July 1991.

[5] X. Ma, P. Wu and H. Shen, "Multifrequency Polarimetric SAR Image Despeckling by Iterative Nonlocal Means Based on a Space-Frequency Information Joint Covariance Matrix," *IEEE J. Sel. Topics Appl. Earth Observ. Remote Sens.*, vol. 12, no. 1, pp. 274-284, Jan. 2019.

[6] V. Battsengel, D. Amarsaikhan, A. Munkh-Erdene, C. Bolorchuluun and C. Narantsetseg, "Application of Multi-Frequency SAR Images for Knowledge Acquisition," *Advances in Remote Sensing*, vol. 2, no. 3, 2013, pp. 242-246.

[7] L. F. Famil, E. Pottier, and J. S. Lee, "Unsupervised classification of multifrequency and fully polarimetric SAR images based on the H/A/alpha-Wishart classifier," *IEEE Trans. Geosci. Remote Sens.,* vol. 39, no. 11, pp. 2332–2342, Nov. 2001.

[8] J. Shi and J. Dozier, "On estimation of snow water equivalence using Sir-C/X-SAR," *Proc. 2nd Int. Workshop Retrieval Bio- Geo-Phys. Parameters SAR Data Land Appl.*, Noordwijk, NL, 1998, pp. 503–510.

[9] B. B. Mandelbrot, *The Fractal Geometry of Nature*. W. H. Freeman, New York, 1983.

[10] G. Franceschetti and D. Riccio, *Scattering, Natural Surfaces and Fractals*. Burlington, MA, USA: Academic, 2007.

[11] G. Di Martino, D. Riccio and I. Zinno, "SAR Imaging of Fractal Surfaces," *IEEE Trans. Geosci. Remote Sens.,* vol. 50, no. 2, pp. 630-644, Feb. 2012.

[12] A. Iodice, G. Di Martino, A. Di Simone, D. Riccio, and G. Ruello, "Electromagnetic Scattering from Fractional Brownian Motion Surfaces via the Small Slope Approximation," *Fractal and Fractional*, vol. 7, no. 5, p. 387, May 2023.

[13] X. Su, C.-A. Deledalle, F. Tupin, and H. Sun, "Two-step multitemporal nonlocal means for synthetic aperture radar images," *IEEE Trans. Geosci. Remote Sens.*, vol. 52, no. 10, pp. 6181–6196, Oct. 2014.

[14] C. A. Deledalle, L. Denis, and F. Tupin, "Iterative weighted maximum likelihood denoising with probabilistic patch-based weights," *IEEE Trans. Image Process.*, vol. 18, no. 12, pp. 2661–2672, Dec. 2009.

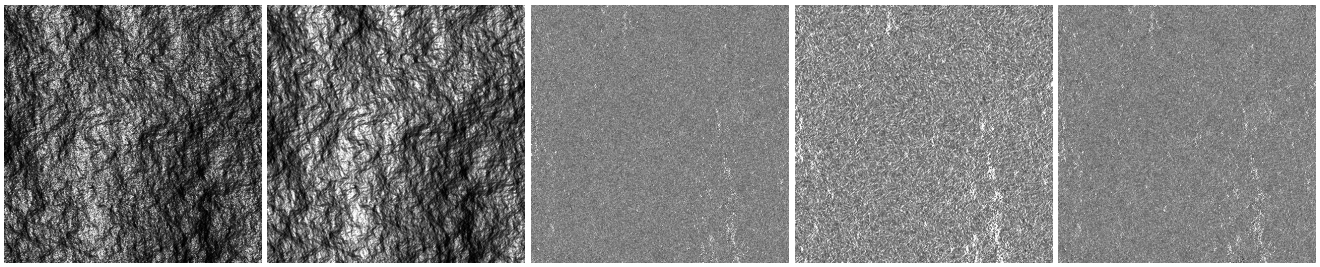

(a) (b) (c) (d) (e)

Fig. 1. 512x512 C-band images: (a) noisy; (b) reference; (c) proposed approach (ratio image); (d) single-channel filtering (ratio image); (e) multi-channel filtering without frequency compensation (ratio image).

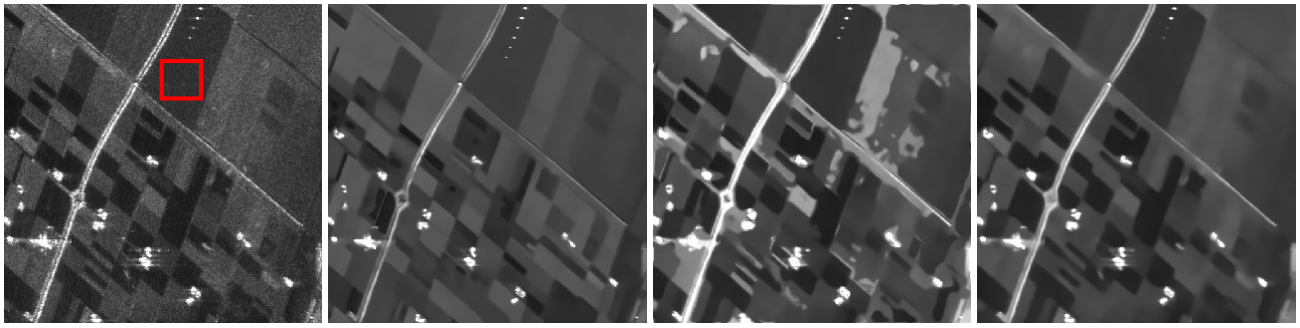

(a) (b) (c) (d)

Fig. 2. 512x512 AIRSAR HH image (P-band): (a) noisy; (b) proposed approach; (c) pure multi-temporal; (d) single-channel. The red box indicates the region used for the evaluation of ENL.

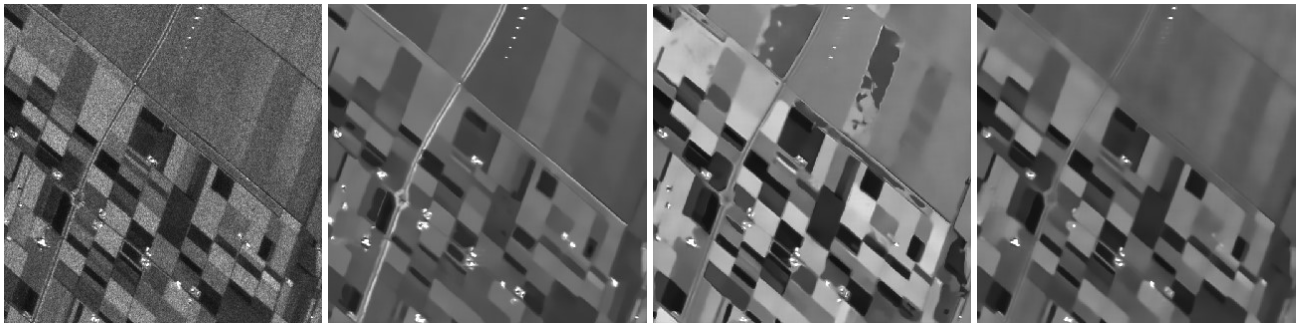

(a) (b) (c) (d)

Fig. 3. 512x512 AIRSAR HH image (L-band): (a) noisy; (b) proposed approach; (c) pure multi-temporal; (d) single-channel.

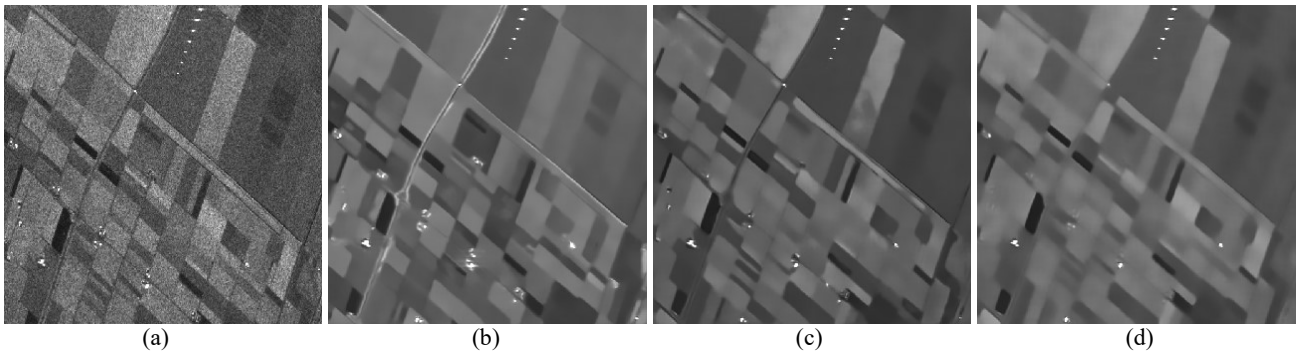

(a) (b) (c) (d)

Fig. 4. 512x512 AIRSAR HH image (C-band): (a) noisy; (b) proposed approach; (c) pure multi-temporal; (d) single-channel.